ELSEVIER

Contents lists available at ScienceDirect

# Acta Biomaterialia

journal homepage: www.elsevier.com/locate/actbio



# Full length article

# Design and validation of a modular micro-robotic system for the mechanical characterization of soft tissues



Andrea Acuna<sup>a</sup>, Julian M. Jimenez<sup>a</sup>, Naomi Deneke<sup>b</sup>, Sean M. Rothenberger<sup>a</sup>, Sarah Libring<sup>a</sup>, Luis Solorio<sup>a,c</sup>, Vitaliy L. Rayz<sup>a</sup>, Chelsea S. Davis<sup>b</sup>, Sarah Calve<sup>a,d,\*</sup>

- <sup>a</sup> Weldon School of Biomedical Engineering, Purdue University, 206 South Martin Jischke Drive, West Lafayette, IN 47907, United States
- b School of Materials Engineering, Purdue University, Neil Armstrong Hall of Engineering, 701 West Stadium Avenue, West Lafayette, IN 47907, United States
- <sup>c</sup> Purdue Center for Cancer Research, Purdue University, 201 South Street, West Lafayette, IN 47906, United States
- d Paul M. Rady Department of Mechanical Engineering, University of Colorado Boulder, 1111 Engineering Center, 427 UCB, Boulder, CO 80309, United States

# ARTICLE INFO

# Article history: Received 7 January 2021 Revised 14 July 2021 Accepted 15 July 2021 Available online 21 July 2021

Keywords: Tensile testing Soft tissue mechanics Tendon mechanics Embryonic tendon Extracellular matrix

# ABSTRACT

The mechanical properties of tissues are critical design parameters for biomaterials and regenerative therapies seeking to restore functionality after disease or injury. Characterizing the mechanical properties of native tissues and extracellular matrix throughout embryonic development helps us understand the microenvironments that promote growth and remodeling, activities critical for biomaterials to support. The mechanical characterization of small, soft materials like the embryonic tissues of the mouse, an established mammalian model for development, is challenging due to difficulties in handling minute geometries and resolving forces of low magnitude. While uniaxial tensile testing is the physiologically relevant modality to characterize tissues that are loaded in tension in vivo, there are no commercially available instruments that can simultaneously measure sufficiently low tensile force magnitudes, directly measure sample deformation, keep samples hydrated throughout testing, and effectively grip minute geometries to test small tissues. To address this gap, we developed a micromanipulator and spring system that can mechanically characterize small, soft materials under tension. We demonstrate the capability of this system to measure the force contribution of soft materials, silicone, fibronectin sheets, and fibrin gels with a 5 nN - 50 µN force resolution and perform a variety of mechanical tests. Additionally, we investigated murine embryonic tendon mechanics, demonstrating the instrument can measure differences in mechanics of small, soft tissues as a function of developmental stage. This system can be further utilized to mechanically characterize soft biomaterials and small tissues and provide physiologically relevant parameters for designing scaffolds that seek to emulate native tissue mechanics.

#### Statement of significance

The mechanical properties of cellular microenvironments are critical parameters that contribute to the modulation of tissue growth and remodeling. The field of tissue engineering endeavors to recapitulate these microenvironments in order to construct tissues *de novo*. Therefore, it is crucial to uncover the mechanical properties of the cellular microenvironment during tissue formation. Here, we present a system capable of acquiring microscale forces and optically measuring sample deformation to calculate the stress-strain response of soft, embryonic tissues under tension, and easily adaptable to accommodate biomaterials of various sizes and stiffnesses. Altogether, this modular system enables researchers to probe the unknown mechanical properties of soft tissues throughout development to inform the engineering of physiologically relevant microenvironments.

© 2021 Acta Materialia Inc. Published by Elsevier Ltd. All rights reserved.

#### 1. Introduction

Biological tissues perform a myriad of functions and vary broadly in composition and mechanical properties. The extracel-

<sup>\*</sup> Corresponding author.

E-mail address: sarah.calve@colorado.edu (S. Calve).

lular matrix (ECM) is an essential component of tissues and is a dynamic network of macromolecules that surrounds cells, regulates cellular behavior, and provides a substrate for tissue organization [1]. The composition of the ECM and interactions between cells and the ECM contribute to the mechanical functionality of tissues [2,3]. Conversely, the mechanical environment is an important factor that drives cellular function and organization [4,5]. Age and disease significantly influence the material properties of biological tissues. Mechanical characterization can assess how these factors change tissue functionality [6,7]. For instance, during tendon development, the composition and organization of the ECM and cells vary widely, which will manifest in changes in the mechanical response of the tissue, such as an increase in tensile strength and tangent modulus [8,9]. Mechanical cues from tissue stiffness, muscle contractions, and embryonic motility support tendon development and changes in material properties (e.g., tangent modulus), which affect the effective transfer of force from muscle to bone, directly impacting functionality [10].

Given the parallels between embryonic development and effective wound healing, understanding how mechanical changes correlate with cell and ECM dynamics during embryonic development can inform tissue engineering and regenerative medicine strategies [11,12]. Mice are commonly used in the study of development and disease due to the ease of genetically modifying the expression of proteins of interest compared to other mammalian species [13–15]. However, embryonic murine tendons are challenging to isolate for uniaxial mechanical testing, therefore tendon development was previously studied using chick models and indentation force curves from tendon cryosections to calculate the moduli at the nano and microscales [16,17]. The microscale indentation moduli increased nonlinearly during development, ranging from ~10-150 kPa, whereas other values reported in the literature for the moduli of late-stage embryonic chick tendon undergoing uniaxial tensile loading varied by about 100-fold, ranging from 0.21 MPa to 20 MPa [10,18], which is likely due to differences in testing modalities. The use of cryosections limits the evaluation of whole-tissue mechanics as a function of development and does not replicate the physiological loading conditions of the tendon in vivo. While cellscale mechanical properties may be more relevant in investigating mechanoregulation of cell differentiation and function, studying the macroscale tensile properties of embryonic tendon is critical for understanding tissue mechanics as a function of develop-

Additionally, in vitro models are a powerful tool to understand the mechanical interactions between cells and the ECM at the fibrillar scale, required to ensure appropriate cell behavior and tissue function [6,19,20]. The use of multifunctional ECM polymers like fibrin and fibronectin provides a framework for evaluating the ECM at the fibrillar scale; however, the mechanical influence of these polymers during tissue growth and remodeling is not completely understood. Fibrin is a temporary matrix that supports blood clotting and wound healing in vivo. Gels can be made in vitro by combining fibrinogen and thrombin, and fibrin gel is used in the clinic as a wound sealant due to its quick polymerization reactions and appropriate tissue adherence. Fibrin gel has also been used as a scaffold in tissue engineering applications [21]. Fibronectin is an ECM protein with many roles, including facilitating cellular adhesion and migration through the ECM, tissue growth and development, and ECM assembly [22]. Under the right conditions in vitro, fibronectin can be polymerized into robust sheets for the 3D culture of cells [23,24]. Characterization of the mechanical properties of embryonic murine tissues and ECM polymers is crucial for understanding the role of mechanics in tissue assembly and providing a benchmark for de novo functional tissue formation and applied regeneration strategies [25,26].

Nevertheless, the mechanical characterization of murine soft tissues and ECM polymers is challenging due to difficulties in handling samples with small dimensions and measuring forces of low magnitudes, making tensile testing equipment used for adult soft tissues unsuitable. Additionally, synthetic hydrogels can be difficult to generate in large geometries to mechanically test using traditional uniaxial tensile testing instrumentation, despite being a critical step in the evaluation of biomaterials [27-29]. Atomic force microscopy (AFM) indentation measurements can be used to mechanically characterize materials and has been utilized to study tissues and hydrogels at the nano and microscales [30]. Using AFM to measure stiffness through compression is a suitable testing modality for hydrogels and other biomaterials designed to withstand compressive forces, for instance, when seeking to recapitulate cartilage. However, many tissues are loaded in tension in vivo, such as tendon, and cells exert tensile forces onto their surrounding microenvironment so that ECM networks and fibrils are uniaxially loaded [31]. The ability to test small, soft tissues and biomaterials in tension while taking force measurements is therefore critical for identifying parameters for regenerative therapies.

Various commercially available and custom-built systems have been developed to uniaxially test small biological materials in tension. The length of small, soft materials that have been tested can range from 500 µm [32] for hydrogels to 20 mm for adult rat Achilles and tail tendon fascicles [33]. The force threshold and resolution that can be measured depend on the sensing mechanism. For example, different uniaxial tensile testing systems used to characterize soft biomaterials or tissues had force resolutions (i.e., the minimum force magnitude that can be measured with a system) ranging from 11 nN [32] to 2.5 mN [34] with force thresholds of at least 100 µN to 2500 µN, respectively. Other commercially available and custom tensile testing systems relevant to biomaterials include: BioTense Bioreactor (Admet) with a 5 N force threshold and 1000 μN resolution; UStretch (CellScale) and Biotester (CellScale) with 0.5 N threshold and 1000  $\mu N$  resolution; Material Testing System developed by Ye et al. [35] with 0.2 N threshold and 100  $\mu N$ resolution; MicroTester (CellScale) with 5 µN threshold and 10 nN resolution. Securing soft biological samples via clamps or winding with wire or thread in order to secure them for testing can result in stress concentrations, increased local deformation proximal to the grips, and low friction between clamps and the sample that can lead to slipping [27,36,37]. Grip-to-grip displacement can be used to calculate strain; however, this does not capture regional variation or account for deformation at the interface between the tissue and the grips. Therefore, strain is commonly calculated by tracking the displacement of the sample of interest using optical surface markers (e.g., microspheres, graphite) [33,38,39] to directly observe sample deformation, avoiding errors attributed to gripping soft biological materials.

Currently available uniaxial tensile testing modalities meet some of these desirable specifications. However, there is no single system that possesses all the necessary criteria to mechanically characterize mouse embryonic tendons. There is a need for an instrument that can measure force at sufficiently high resolution, optically measure sample deformation, keep samples hydrated throughout testing, and effectively secure the minute geometries of embryonic mouse tendons and other small, soft tissues and biomaterials. To address this gap, we developed a system that satisfies all these criteria. We designed and 3D printed springs and fabricated sample holding frames to accommodate a range of sample geometries and stiffness. The spring was coupled with a commercially available micromanipulator and force sensors (FemtoTools) that have 100 µN threshold with 5 nN resolution,  $10{,}000~\mu N$  threshold with 5  $\mu N$  resolution, and  $100{,}000~\mu N$  threshold with 50 µN resolution (depending on the sensor used and the data acquisition rate), and with a dissecting microscope to visu-

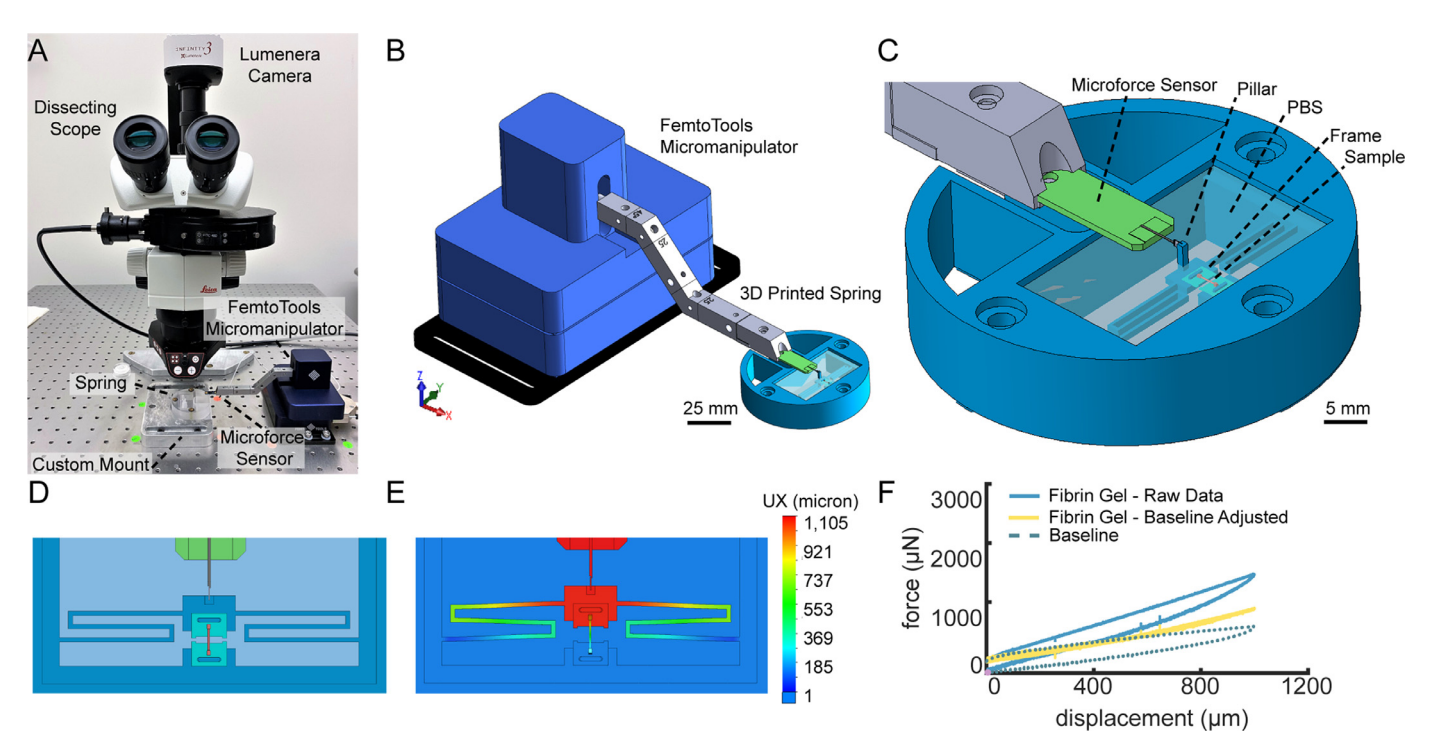


**Fig. 1. Instrumentation to measure force and optical displacement of soft tissues.** (A) Dissecting microscope and mechanical testing system. (B) FemtoTools micromanipulator and spring assembly. (C) Detail of spring assembly. The microforce sensor has a custom hook probe that connects the micromanipulator to the spring, enabling the samples to remain hydrated in PBS. Samples are glued onto frames and loaded onto the spring. The sides of the frame are cut prior to testing. Top view of SolidWorks model of sample before (D) and during (E) tensile testing. (F) Fibrin gel raw data, baseline, and baseline-adjusted force-displacement curves demonstrate the ability of the system to measure the force contribution of soft materials. At a displacement of 1000 μm, the force values for the raw fibrin gel, the baseline adjusted fibrin gel, and the baseline were 1478 μN, 899 μN, and 579 μN, respectively. At a 1000 μm displacement, the raw fibrin gel force was 155% greater than the respective baseline value at the same displacement.

alize sample deformation. The FemtoTools system was chosen because it provides force thresholds and resolutions comparable to other commercially available tensile testing modalities relevant to biomaterials. Additionally, the modularity of the FemtoTools system allowed us to adapt our system to accommodate different sample sizes and stiffnesses. The system was validated by comparing the measured mechanical response of Solaris silicone, a material with known mechanical properties, to the mechanical response of the same material measured with a commercially available tensile tester. Our system measured the mechanical responses of soft materials of varying stiffnesses and geometries, including fibronectin sheets, and fibrin gels, as well as assess mouse embryonic tendon mechanics as a function of development. This system can be further utilized to mechanically characterize other tissues and ECM, which is critical for expanding the understanding of the cellular microenvironment during growth and development and defining design parameters for scaffolding with applications in regenerative medicine.

#### 2. Materials and methods

#### 2.1. Development of modular tensile testing system

The micromechanical testing assembly was built around a dissecting microscope (M80, Leica Microsystems; Fig. 1A). A commercially available micromanipulator system (FT-RS1002, FemtoTools) and force sensing probes (FT-S10'000 and FT-S100'000, FemtoTools) were adapted for uniaxial loading of small soft tissues and biomaterials (Fig. 1B). The micromanipulator system maneuvers along the x, y, and z axes with a displacement range of 5 nm – 26 mm. The microforce sensing probes are capable of resolving 5 nN – 50  $\mu$ N forces. The micromanipulator and each individual microforce sensor were calibrated by the manufacturer prior to use.

The displacement of the micromanipulator was verified optically under a dissecting microscope. The microforce sensors have exposed electronics that will be damaged when they come in contact with aqueous solutions. Therefore, springs were designed to enable samples to remain hydrated during testing, while providing an attachment point for the microforce sensor away from the liquid. Custom springs and frames (Fig. 1C) were designed and fabricated to accommodate the mechanical testing of samples with varying geometries and stiffnesses. Three spring configurations, spring 1, spring 2, and spring 3, were designed to accommodate different sample geometries by varying the distance between fixed and moveable ends (Supplemental Fig. 1). The distance between the fixed and moveable end was 2 mm, 3.7 mm, and 8.5 mm for spring 1, spring 2, and spring 3, respectively. Frames were drawn in Adobe Illustrator (Adobe) and laser cut out of 100 µm-thick polyethylene terephthalate (PET) using a Universal Laser VLS3.50 (Universal Laser Systems) (Supplemental Fig. 2A-H). The PET frames kept the samples in a static configuration and minimized sample deformation while staining, processing, and mounting onto the 3D printed springs. The spring and micromanipulator assembly were securely mounted onto an optical table using custom-built fixtures to avoid undesired part movement during testing and consequent system damage. The dissecting microscope, also securely mounted on the optical table, facilitated handling and situating samples on the 3D printed spring and enabled the calculation of optical strain.

Springs were designed using SolidWorks (Dassault Systèmes), 3D printed (ProJet MJP 2500) with UV curable plastic (M2R-CL, VisiJet), and post-processed to remove wax support material by placing first in a steam bath then a heated oil bath, following the manufacturer's guidelines. The resolution of the printer is  $32 \times 28 \times 32 \ \mu\text{m}^3$ . A liquid-retention basin was incorporated into the spring design to keep samples hydrated with  $1 \times \text{phosphate}$  buffered saline (PBS) throughout testing. The spring was

connected to the micromanipulator system via a pillar that vertically offset the microforce sensor, away from the PBS, to minimize risk of damaging exposed electronics (Fig. 1C). The resolution of the 3D printer was not sufficient to create an interface onto which the hook at the end of the microforce sensor probe could attach. Therefore, a small PET hook-interface was laser cut and adhered onto the spring at the top of the pillar using Loctite Super Glue Gel Control (cyanoacrylate-based adhesive). The PET hook-interface was designed to facilitate attachment to the hooked probe at the end of the microforce sensor (Fig. 1C). The initial force-displacement measurement was compared to other springs to confirm the mechanical response was within the expected magnitude.

#### 2.2. Mechanical Testing Protocol

PBS was added to the liquid-retention basin of the spring at least 2 hours prior to mechanical tests. PET frames containing the samples to be tested were manually loaded onto the spring and cut with angled scissors prior to mechanically testing (Supplemental Fig. 2A-H), freeing the sample to deform under tension. (Fig. 1C-E). The length of each sample was measured optically and was used to calculate the appropriate speed to achieve the desired strain rate. Custom LabVIEW programs were written to control the movement of the micromanipulator and to automate testing by prescribing the direction, magnitude, and speed of displacement. Force measurements and actuator displacement were recorded at 100Hz. Force-displacement curves were used to demonstrate the capability of the system to measure the force response of soft materials. To further characterize the stress-strain response of certain specimens, strain and cross-sectional area were measured optically.

To enable the optical measurement of engineering strain, fiducial lines were photobleached onto AF488 labeled specimens using an upright Zeiss LSM 800 confocal microscope (Carl Zeiss Microscopy) and a 10 × Plan-Neofluar (NA = 0.3) objective. Equidistant lines were photobleached by creating a 20 µm wide region of interest (ROI) along the sample width using the *Crop* feature in the ZenBlue software package (Carl Zeiss Microscopy). The power of the 488 laser was set to 100% and a line was photobleached into the AF488 stained samples by acquiring a z-stack through the sample thickness in 10 µm increments. After the photobleached lines were generated, a z-stack of the entire sample was acquired (Supplemental Fig. 2I-K). The unloaded cross-sectional area was measured between each pair of fiducial lines from the z-stack acquired using the ZenBlue software package (Carl Zeiss Microscopy).

The dissecting microscope magnification was adjusted to enable visualization of the sample throughout testing and a camera (INFINITY3-3URC, Lumenera) was coupled to the microscope to acquire videos for the duration of a mechanical test. For 2.5  $\times$  magnification, the ROI during video acquisition was 6.2 mm  $\times$  4.7 mm and 1936  $\times$  1456 pixels. The exposure time was adjusted for each sample to optimize contrast between the sample and fiducial lines using the camera's software package (INFINITY ANALYZE 6.5, Lumenera). Frame rate is inversely proportional to exposure time. Since the exposure time was adjusted for each sample based on fluorescence intensity, the frame rate ranged from 3 - 8 frames/second.

The spring and sample were loaded in parallel (Fig. 1C). Parallel force contributions are additive, i.e.,  $F_{combined} = F_{spring} + F_{sample}$ . Therefore, to isolate the force contribution of the sample, the contribution of the spring, or baseline, was measured prior to every test by recording force-displacement data of the spring in the system without a sample (Fig. 1F). A baseline was recorded for each individual sample at the appropriate strain rate (based on the sam-

ple length) and to account for potential variation in the force contribution of the spring over time.

#### 2.3. Data analysis

After tensile testing was completed, the baseline force readings (i.e., spring alone) were subtracted from the force recorded for each sample to isolate the force contribution of the material of interest (i.e.,  $F_{sample} = F_{combined} - F_{spring}$ ). To calculate stress, the isolated force for each sample was divided by the cross-sectional area. The FIJI (NIH) getSplineCoordinates macro was modified and used to manually draw segmented polylines over the fiducial lines on each frame from the recorded video. Each polyline was converted into a smoothed spline, and the x and y position of each point along the splines was output as an array on a .txt file. A custom MAT-LAB (MathWorks) algorithm was written to import the output arrays from FIJI and calculate the average distance between fiducial lines for each frame from the recorded video using the x and y coordinates from the FIJI output. Optical strain was calculated using the equation  $(L_i - L_0)/L_0$ , where  $L_0$  is the average distance between fiducial lines for the first frame of the video, and Li is the average distance between fiducial lines for each subsequent frame (Supplemental Fig. 3).

The acquisition rate for force measurement was 100 data points per second (100Hz), and videos were recorded at 3 – 8 frames per second. Therefore, the stress data arrays were larger and contained more time intervals than the strain data arrays. To generate stress-strain curves, a time array was generated using the strain data. Then, stress values which corresponded to the strain time points were selected. The corresponding stress and strain data were plotted and fit to a polynomial function using Excel curve fitting algorithms, based on R<sup>2</sup> values, ensuring the polynomials followed the typical stress-strain responses of soft tissues [40,41]. The derivative of the polynomial function at a specific strain value was used to calculate the tangent moduli at selected strains.

# 2.4. Sample preparation

#### 2.4.1. Reference material - Solaris silicone

System validation was performed by testing Solaris (Smooth-On, Inc.), a platinum-cured silicone, and comparing data from our setup with that acquired using a commercially available bulk tensile tester (TA.XTPlus Connect, Stable Micro Systems). Solaris was selected because it has well defined material properties that can be modulated to be similar to the biological samples of interest [27,42,43]. Solaris was prepared per manufacturer's instructions and cut to size manually with a scalpel blade. A mixture of equal parts Solaris Part A and Part B was prepared in a 20 mL scintillation vial followed by degassing with a vacuum desiccator. Thin film samples for mechanical testing on the FemtoTools system were prepared by spin coating (Laurell Technologies Corporation WS-650-23B) 2 g of uncured Solaris on a 75 mm × 25 mm microscope slide coated with polyacrylic acid, which served as a sacrificial layer. Samples were spin coated at 3000 RPM for 30 seconds then placed in an oven at 70°C to cure for 3 hours. The films were removed from the microscope slide by dissolution of the intermediate polyacrylic acid layer using reverse osmosis purified water. To generate samples with the optimal aspect ratio (length:width  $\geq$ 5:1) for tensile testing, the thin films were cut using a laser-etched grid and a scalpel [44,45]. The resulting dimensions were measured optically from images acquired with a dissecting microscope. Samples tested with spring 1 were 2645.0  $\pm$  471.4  $\mu m$   $\times$  216.4  $\pm$ 42.3  $\mu m$  (n = 5) and samples tested with spring 2 were 3514.0  $\pm$ 420.6  $\mu m \times$  308.1  $\pm$  82.5  $\mu m$  (L  $\times$  W) (n = 5), all with a thickness of 117.0  $\pm$  4.2  $\mu$ m. Solaris thin films were adhered directly

to PET frames using Loctite Super Glue Gel Control (Supplemental Fig. 2E). Tensile tests were performed using the FemtoTools micromanipulator and spring system described above, while the samples were surrounded by PBS. Tensile tests were conducted using spring 1 and spring 2. Actuator displacement data was used to calculate strain.

#### 2.4.2. Bulk material testing – Solaris silicone

Samples for bulk testing were prepared by filling a 75 mm  $\times$  50 mm  $\times$  4 mm glass mold with uncured Solaris and leaving it to cure in an oven at 70°C for 5 hours. The dimensions of samples tested on the bulk tensile tester were 15.29  $\pm$  0.48 mm  $\times$  6.32  $\pm$  1.50 mm  $\times$  3.85  $\pm$  0.04 mm (L  $\times$  W  $\times$  H) (n = 5). For bulk testing, Solaris samples were gripped at each end using the TA.XTPlus clamps, and tensile tests were performed at a strain rate of 0.01 s<sup>-1</sup> while force and displacement data were recorded through the TA.XTPlus Connect system. These tests were performed in the ambient environment (i.e., dry) as it was not possible to add a hydration chamber around the TA.XTPlus Connect.

#### 2.4.3. Fibrin gels

Porous polyethylene blocks were adhered onto 6 mm × 12.5 mm frames using Loctite Super Glue Gel Control and used as anchor points for 2 mg/mL fibrin gel constructs (Supplemental Fig. 2F). A custom mold was used to align the frame and to control the shape of fibrin gel as it polymerized so that a rectangular gel formed between the two porous polyethylene blocks. Human fibrinogen (14.15 mg/mL; FIB3, Enzyme Research Laboratories) and Alexa Fluor 488 conjugated human fibrinogen (1 mg/mL; F-13191, Molecular Probes) were thawed in a 37°C water bath, mixed at a 1:10 fluorescent to non-fluorescent fibringen content ratio, and diluted in PBS to achieve a 2 mg/mL fibrinogen solution. Next, 1 μL 2M CaCl<sub>2</sub> was added to the fibringen solution to increase gel rigidity and stability [46,47]. Human  $\alpha$ -thrombin (HT 1002a, Enzyme Research Laboratories) was thawed, diluted to 1 U/μL, and added to the 2 mg/mL fibrinogen solution at a concentration of 0.0004 U thrombin per mg fibrinogen to initiate polymerization of the fibrin gel. Fiducial lines were photobleached and crosssectional areas were measured as described above using a STEL-LARIS 5 confocal microscope (Leica Microsystems) and a 10x Apochromatic dry (NA = 0.40) objective were used. Frames with fibrin gels (n = 5) were loaded onto spring 3, and tensile tests were conducted at 0.01  $s^{-1}$  strain rate and prescribing a 1000  $\mu m$  - 6000  $\mu m$  displacement, equivalent to  $\varepsilon = 0.15$  – 0.91 based on actuator displacement. Samples were kept hydrated by PBS in the liquidretention basin during testing.

# 2.4.4. Fibronectin

Polydimethylsiloxane (Sylgard 184, Dow Corning) was cured at a 10:1 elastomer to curing agent ratio, manually cut into 1 mm  $\times$  1mm  $\times$  1 mm blocks, adhered onto 6 mm  $\times$  12.5 mm PET frames using Loctite Super Glue Gel Control, and coated with fibronectin sheet as previously described (Supplemental Fig. 2G) [23,48]. To visualize the samples, fibronectin-coated frames were stained with Alexa Fluor 488-conjugated wheat germ agglutinin (WGA; ThermoFisher), diluted 1:100 in 1  $\times$  PBS + 0.2% bovine serum albumin + 0.02% sodium azide for 24 hours at 4°C, then rinsed with 0.1% Triton X-100 in 1  $\times$  PBS (PBST) at room temperature for 30 minutes. Fibronectin-coated frames (n = 2) were loaded onto spring 3 for uniaxial loading and surrounded by PBS during testing. Cyclic loading was performed to 400  $\mu$ m at a strain rate of 0.04 s $^{-1}$  for 10 cycles. Tensile test to failure was conducted at 0.04 s $^{-1}$ .

#### 2.4.5. Developing tendons

All murine experiments were approved by the Purdue Animal Care and Use Committee (PACUC; protocol 1209000723). PACUC

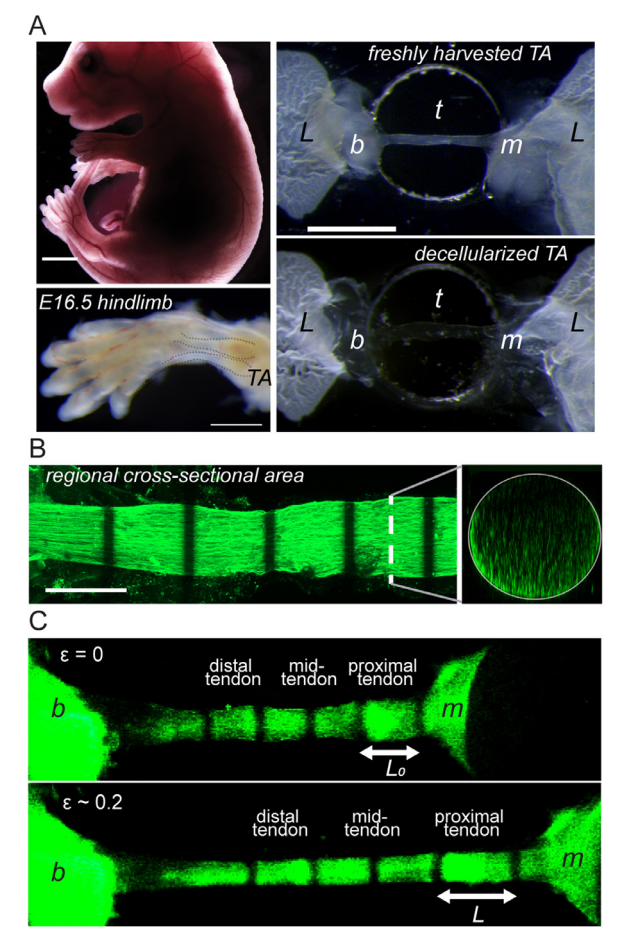


Fig. 2. Isolation and preparation of E16.5 murine tendon for tensile testing. (A) The TA muscle – tendon – bone units were carefully dissected from freshly harvested embryos. To minimize damage to the tendon (t) during processing as well as to attach them to the 3D printed spring part during mechanical testing, muscle – tendon – bone units were glued onto PET frames using Loctite (L) at the muscle (m) and the bone (b) insertions (bars = 1 mm). (B) Tendons were stained with AF488-conjugated wheat germ agglutinin, and photobleached with a Zeiss 800 confocal to obtain fiducial lines for optically measuring strain. Full-thickness z-stacks were obtained to enable quantification of the cross-sectional area (bar = 200  $\mu$ m). (C) Full field images of E16.5 decellularized TA tendon at  $\varepsilon$  = 0.0 and 0.2 showing the regions investigated along the tendon.

ensures that all animal programs, procedures, and facilities at Purdue University adhere to the policies, recommendations, guidelines, and regulations of the USDA and the United States Public Health Service in accordance with the Animal Welfare Act and Purdue's Animal Welfare Assurance. C57BL/6 mice were time-mated to generate embryonic day (E)16.5 and E18.5 embryos. Dams were euthanized via CO<sub>2</sub> inhalation, which was confirmed using cervical dislocation. Embryos were removed from the uterine horns, rinsed in chilled 1  $\times$  PBS and the hindlimbs were excised at the hip joint. Tibialis anterior (TA) muscle-tendon-bone units were dissected by removing the skin with tweezers and then the surrounding connecting tissue with a blade under a dissecting microscope to avoid tissue damage. The bone and muscle insertions were maintained to keep the physiologically relevant boundary conditions of the tendons and aid in sample handling for mechanical testing. Tendons were adhered directly to laser-cut PET frames at the bone and muscle insertions using Loctite Super Glue Gel Control (Fig. 2A; Supplemental Fig. 2H) and were immediately immersed in a large volume of PBS. Direct contact between the tendons and glue was avoided to prevent altering the composition of the tendons. Samples were either stained immediately as follows or decellularized

as described below. Tendons were rinsed in 1  $\times$  PBS and stained with AF488-conjugated WGA (ThermoFisher) to visualize proteoglycans, diluted 1:50 in blocking buffer [10% donkey serum (Lampire) in 1  $\times$  PBST] for 1 hr at room temperature.

Samples were mounted onto the springs and kept hydrated with PBS at all times. Fiducial lines were photobleached and cross-sectional areas were calculated, as described above (Fig. 2B). E16.5 tendons were tested using 4 mm  $\times$  6 mm frames and spring 1 (n = 3), while E18.5 tendons were tested using 4 mm  $\times$  7.65 mm frames and spring 2 (n = 3) (Supplemental Fig. 1C). Tensile tests to failure were conducted at 0.01 s $^{-1}$  strain rate without preconditioning. Stress-strain datapoints were fit to polynomial functions for the calculation of the tangent moduli at relevant strain values. Embryonic tendon data sets were fit to a second order polynomial with the y-intercept set at the origin.

#### 2.4.6. Decellularization of tendons

E16.5 and E18.5 TA muscle-tendon-bone units, secured to PET frames, were incubated in 8 mL 0.05% sodium dodecyl sulfate (SDS) with 1  $\times$  Halt protease inhibitor (PI, ThermoFisher) in 1 × PBS and gently rocked overnight. Completion of decellularization was determined by subjective visual inspection of samples and when ECM visualization was enhanced after immunostaining [49,50]. Upon decellularization, samples were rinsed in an excess of 1 × PBS for 1 hr and stained and imaged prior to mechanical testing as described above. Tensile tests were conducted at 0.01 s<sup>-1</sup> strain rate and loading by prescribing either a 5,000 µm displacement, a displacement equivalent to 100% strain based on actuator displacement, or until material failure. Samples were hydrated with PBS at all stages of testing. The regional stress-strain response corresponding to an individual pair of lines was averaged along the entire sample to investigate the effect of decellularization on E16.5 tendons and compare the mechanics of decellularized E16.5 (n = 3) and E18.5 (n = 3) embryonic timepoints (Fig. 2C). The purpose of testing decellularized tendons was twofold: to isolate and study the contribution of the ECM to the mechanics of embryonic tendons and investigate if our system can resolve differences in mechanical properties as a function of treatment (i.e., decellularization) by testing both untreated and treated tendons.

# 2.5. Statistical methods

All the statistical analyses were conducted using GraphPad Prism 8.4.2 (GraphPad Software). A two-way ANOVA and Tukey's post hoc test were performed to evaluate differences in the mean tangent moduli between Solaris samples tested with different instruments (i.e., custom FemtoTools system and TA.XTPlus Connect). To evaluate tendon mechanics as a function of decellularization, residuals were checked for normality and Gaussian distribution. Residuals did not pass Shapiro-Wilk and D'Agostino-Pearson omnibus tests, so a two-way ANOVA was performed on the log<sub>10</sub> of the tangent moduli. For the evaluation of tendon mechanics as a function of development, a two-way ANOVA with Sidak multiple comparisons was conducted on the mean tangent moduli at each stage. For the evaluation of regional stiffness in E16.5 tendons, a two-way ANOVA and Tukey's post hoc test was performed.

#### 3. Results

#### 3.1. Spring Design

A commercially available FemtoTools micromanipulator system was adapted to enable the optical measurement of strain while keeping biological samples hydrated in a bath. To mitigate the risk of damaging the microforce sensing probe with the PBS used to keep samples hydrated, 3D printed springs were designed. Three

different springs were designed to accommodate various sample geometries (Supplemental Fig. 1). Custom PET frames for each spring were laser cut and used to secure the samples while processing and mounting onto the spring. The coil design for springs 1-3 was the same; however, the spacing between the frame attachment sites were modified to accommodate the geometry of the different frames and biological samples. The spacing between the fixed and moveable sections of the spring were 2 mm, 3.7 mm, and 8.5 mm for spring 1, spring 2, and spring 3, respectively.

The spring and sample are loaded in parallel (Fig. 1D). Forces in parallel are additive, i.e.,  $F_{combined} = F_{spring} + F_{sample}$ . Therefore, the force contribution from the spring alone (baseline) was subtracted to isolate the force contribution from the sample ( $F_{sample} = F_{combined}$ -  $F_{spring}$ ; Fig. 1F). The force necessary to deform the three different spring designs was comparable; the force responses (tangent of the loading curve at a 250 µm displacement) of spring 1, spring 2, and spring 3 for a 1000 μm displacement at 10μm/s were 0.61 μN/μm,  $0.67 \mu N/\mu m$ , and  $0.62 \mu N/\mu m$ , respectively (Supplemental Fig. 4A). The stiffness of the spring was higher immediately after 3D printing and post-processing, with an initial force response (tangent of the loading curve at a 250 μm displacement) of 2.84 μN/μm. However, as the spring was loaded and unloaded over time, the stiffness decreased and reached a stable force response (Supplemental Fig. 4B). From days 0 - 7, there was a cumulative loading displacement of 2.1 mm, and the force response of spring 1 ranged from 2.88  $\mu$ N/ $\mu$ m to 0.58  $\mu$ N/ $\mu$ m, the average and standard deviation were 1.72  $\pm$  0.96  $\mu$ N/ $\mu$ m. From weeks 5 – 21, there was a cumulative loading displacement of 275.0 mm, and the force response of spring 1 ranged from 0.61 μN/μm to 0.41 μN/μm, the average and standard deviation were 0.51  $\pm$  0.09  $\mu$ N/ $\mu$ m. The trend in decreasing standard deviation as spring 1 was loaded and unloaded over time, suggests that the spring will reach a fatigue limit with use and settle to a constant force response. The variation in the initial stiffness of the spring serves to highlight the importance of why the baseline contribution was measured prior to testing samples to account for the force contribution from the springs.

Adding PBS to the liquid-retention basin led to a consistent effect on the mechanical response of the spring. The stiffness of the spring was higher when dry than when immersed in PBS. The initial stiffness (tangent at 250 µm displacement), from two measurements taken 7 minutes apart, was 2.34  $\pm$  0.02  $\mu N/\mu m$ . After the spring was exposed to PBS for approximately 90 minutes, the stiffness decreased to  $0.66 \pm 0.01 \, \mu\text{N/\mu}\text{m}$ , whereas 994 minutes later, the stiffness remained unchanged 0.64  $\pm$  0.02  $\mu N/\mu m$  (Supplemental Fig. 5). Therefore, the spring should be placed in PBS at least 90 minutes prior to mechanical testing to achieve a stable baseline. Once a baseline force response was established, the force response of the spring did not significantly change before and after sample testing (p = 0.32, Student's t-test). The pre-test baseline stiffness of the spring (tangent at 250  $\mu m$  displacement) was 0.61  $\pm$  0.02  $\mu N/\mu m$  (n = 3). Post-test baselines were recorded after testing fibrin gel samples and the spring stiffness was 0.58  $\pm$  0.05  $\mu$ N/ $\mu$ m (n = 3; Supplemental Fig. 6).

#### 3.2. Validation of spring-micromanipulator system

To confirm that the system could accurately determine the stress-strain response of a material of known properties, Solaris, a platinum-cure silicone rubber, was tested using both our system and a commercially available tensile-tester, TA.XTPlus Connect. Furthermore, two different spring configurations, spring 1 and spring 2, which have the same spring geometry, but were designed to test materials of different lengths (Supplemental Fig. 1), were compared to investigate if variations in design influenced the characterization of the material properties. Representative curves from the three configurations qualitatively showed sim-

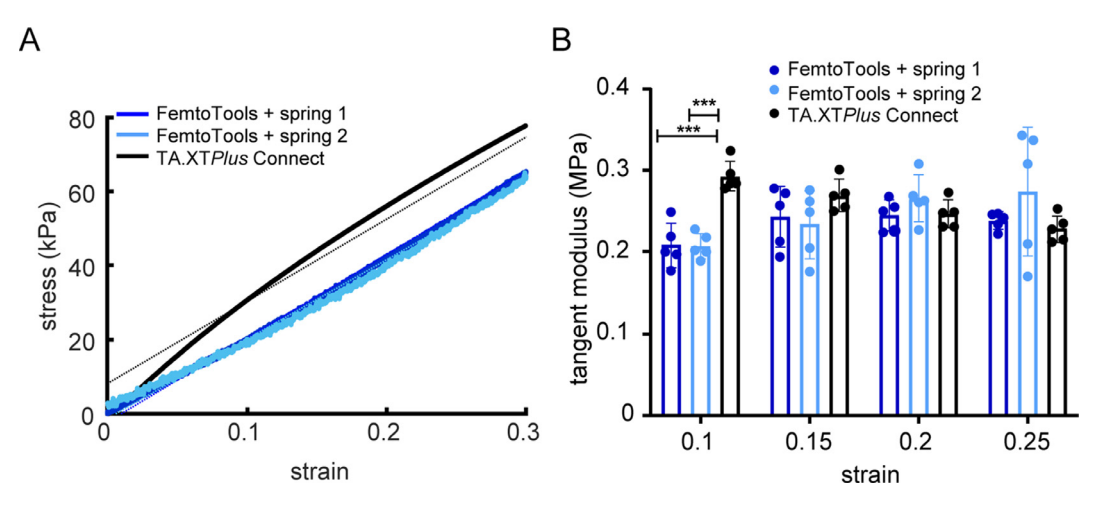


**Fig. 3. Validation of FemtoTools micromanipulator system.** Solaris silicone samples were tested using our FemtoTools system with two different spring configurations and a TA.XTPlus Connect bulk material testing instrument. (A) Representative stress-strain curves of Solaris samples on the two instruments. The dotted line is a linear curve fitting of the Solaris sample tested on the TA.XTPlus Connect. (B) Comparison of the tangent moduli of Solaris tested on the FemtoTools system and TA.XTPlus Connect (FemtoTools + spring 1 (n=5), FemtoTools + spring 2 (n=5), TA.XTPlus Connect (n=5); error bars = std. dev.; two-way ANOVA, followed by Tukey's post hoc test: \*\*\*p<0.0002, \*\*\*\*p<0.0001).

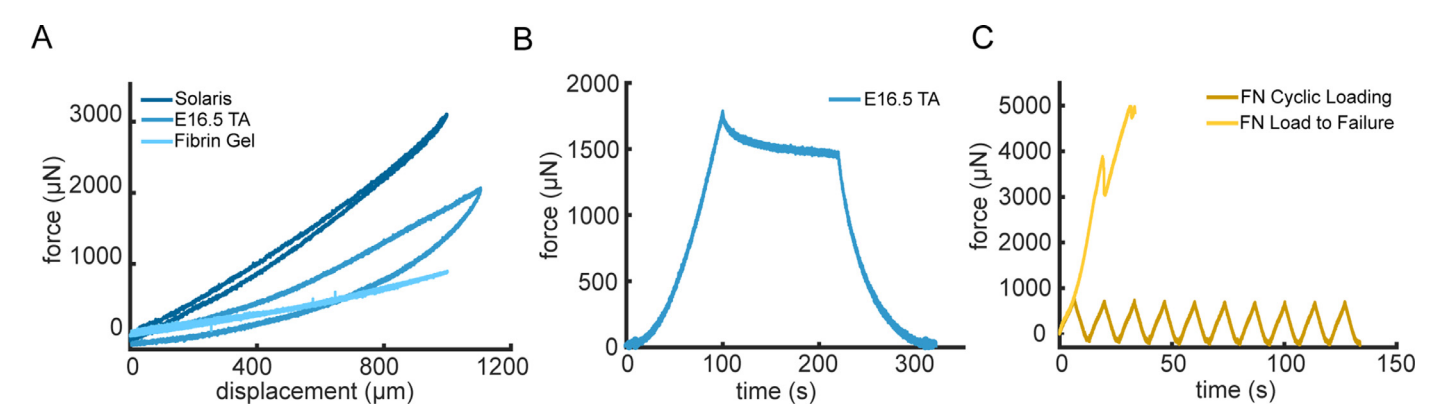


**Fig. 4. Resolution of the mechanics of soft tissues and biomaterials in response to a variety of tests.** Baseline-adjusted curves. (A) Tensile loading and unloading curves of Solaris, E16.5 TA tendon, and fibrin gel. At a 1000 μm displacement during loading, the baseline adjusted force values for Solaris, E16.5 TA tendon, and fibrin gel were 3110 μN, 1786 μN, and 899 μN, respectively. At 1000 μm displacement, the raw force values of Solaris, E16.5 tendon, and fibrin gel were 407%, 282%, 155% greater than their respective baselines at the same displacement values. (B) Stress relaxation test for E16.5 TA tendon. (C) Cyclic loading and tensile loading to failure for fibronectin (FN) sheet. At 16.7 seconds (equivalent to 1000 μm displacement), the baseline adjusted force value for fibronectin was 3256 μN, this was 292% greater than the respective baseline force value at the same time.

ilar stress-strain responses (Fig. 3A); however, the slope was larger by 29% at  $\varepsilon = 0.1$  for samples tested with the TA.XTPlus instrument. Quantification of the tangent moduli showed no significant difference between the two spring configurations, while the stressstrain response of the bulk material diverged from these values at lower strains (Fig. 3A). This divergence was indicated at  $\varepsilon = 0.1$ , where the tangent moduli of Solaris samples tested with Femto-Tools (spring 1: 0.208  $\pm$  0.024 MPa; spring 2: 0.207  $\pm$  0.014 MPa) were significantly different than those tested with the TA.XTPlus system (0.293  $\pm$  0.016 MPa) (Fig. 3B). Testing Solaris on spring 1 and spring 2 with the FemtoTools system did not lead to significantly different tangent moduli for this material. At strain values of 0.15 (FemtoTools spring 1: 0.243  $\pm$  0.033 MPa; FemtoTools spring 2: 0.234  $\pm$  0.037 MPa; TA.XTPlus: 0.269  $\pm$  0.018 MPa), 0.2 (FemtoTools spring 1: 0.245  $\pm$  0.017 MPa; FemtoTools spring 2: 0.266  $\pm$  0.026 MPa; TA.XTPlus: 0.246  $\pm$  0.015 MPa), and 0.25 (Femto-Tools spring 1: 0.238  $\pm$  0.009 MPa; FemtoTools spring 2: 0.274  $\pm$ 0.070 MPa; TA.XTPlus: 0.229  $\pm$  0.015 MPa) there were no significant differences in the tangent moduli obtained for Solaris with all 3 different testing configurations. Using the FemtoTools system with both spring 1 and spring 2 yielded comparable results to the tangent moduli of Solaris measured by the TA.XTPlus tensile tester. This validation verifies the capability of the system to accurately characterize the material properties of samples using either spring.

#### 3.3. Uniaxial loading of various materials

The versatility of the system was demonstrated by uniaxially testing a variety of soft materials, specifically fibrin gels, sheets of fibrillar fibronectin, and embryonic murine TA tendons. The forcedisplacement response of these disparate samples can be clearly resolved after subtracting the baseline contribution of the spring (Fig. 4). At a 1000 µm displacement during loading, the baseline adjusted force values for Solaris, E16.5 TA tendon, and fibrin gel were 3110  $\mu N$ , 1786  $\mu N$ , and 899  $\mu N$ , respectively. At 1000  $\mu m$  displacement, the raw force values of Solaris, E16.5 tendon, and fibrin gel were 407%, 282%, 155% greater than their respective baselines at the same displacement values. At 16.7 seconds (equivalent to 1000 µm displacement), the baseline adjusted force value for the fibronectin sheet was 3256 µN, this was 292% greater than the respective baseline force value at the same time. Additionally, our system was able to perform a variety of mechanical tests and measure different mechanical responses. For instance, Solaris and E16.5 TA tendon displayed viscoelastic properties, as observed

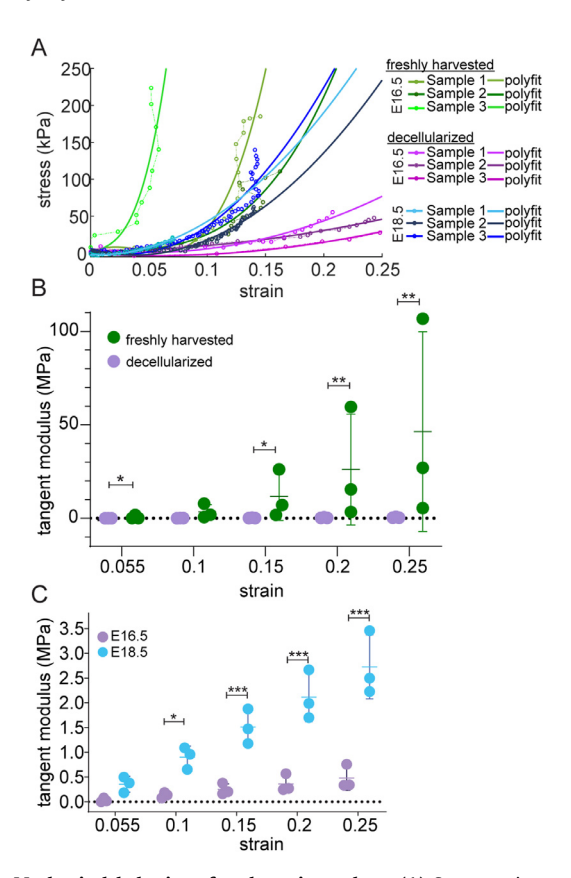


**Fig. 5. Mechanical behavior of embryonic tendons.** (A) Stress-strain curves for freshly harvested E16.5 tendons (green), and decellularized E16.5 (purple) and E18.5 (blue) samples, along with the fitted polynomials. (B) Tangent moduli of freshly harvested and decellularized E16.5 tendons were significantly different. (Sidak multiple comparisons: \*0.0021 <  $p \le 0.0332$ ; \*\*0.0002 <  $p \le 0.0021$ ; n = 3; error bars = std. dev.) (C) The tangent moduli of decellularized tendons at E18.5 were significantly greater than those harvested at E16.5 for  $\varepsilon \ge 0.1$ . (Sidak multiple comparisons: \*0.0021 <  $p \le 0.0332$ ; \*\*0.0002 <  $p \le 0.0021$ , \*\*\*0.0002 <  $p \le 0.0001$ ; n = 3; error bars = std. dev.)

by the hysteresis in tensile test (Fig. 4A) and stress relaxation curves (Fig. 4B). In contrast, the fibrin gel was elastic (Fig. 4A). The fibronectin sheet demonstrated the ability of the system to perform cyclic loading and loading to failure (Fig. 4C). We previously reported that the average tangent modulus of these fibronectin sheets tested using the same system was 0.63  $\pm$  0.34 MPa at  $\varepsilon$ =0.25 [23]. Conversion of the force-displacement curves of 2 mg/mL fibrin gels to stress and strain determined that the average tangent modulus at  $\varepsilon$ =0.25 was 0.15  $\pm$  0.08 MPa (n = 5; Fig 4A is a representative force – displacement curve of one of the five samples).

# 3.4. Stress-strain evaluation of embryonic murine tendon ECM

To demonstrate that our system can resolve differences in mechanics of small, soft tissues as a function of developmental stage, we investigated how embryonic tendon mechanics vary due to development and cellularity. The regional stress-strain response (i.e., corresponding to an individual pair of photobleached lines) was averaged along the entire sample to compare E16.5 and E18.5 embryonic timepoints. The tangent moduli calculated at different strains for each sample were plotted for both developmental timepoints (Fig. 5A). To isolate the mechanical contribution of cells and the ECM of developing tendons, we decellularized tendons and compared the stress-strain response to freshly harvested tendons. The evaluation of E16.5 tendons showed decellularization had a significant effect on the tangent moduli according to a two-way ANOVA.

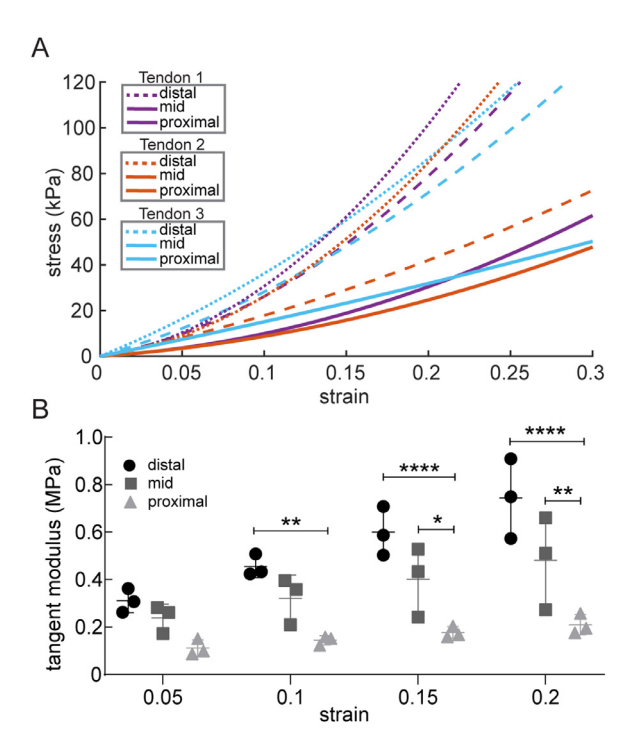


**Fig. 6. TA tendons show regional variability at E16.5.** (A) Polynomial fits of the stress-strain response of decellularized E16.5 TA tendons at different regions. (B) Tukey multiple comparisons showed significant differences in the tangent moduli between individual groups (\*0.0021 ; \*\*0.0002 <math>, \*\*\*\*0.0002 <math>, \*\*\*\* <math>> 0.0001, \*\*\*\* > 0.0001, \*\*\*\*0.0001 , \*\*\*\*0.0001 <math>, \*\*\*0.0001 <math>, \*\*\*0.0001

Multiple comparisons showed significant differences between individual groups except at  $\varepsilon=0.1$ , potentially due to the large variability in the dataset, the sample size, and the efficacy of the decellularization method to remove all cellular components (Fig. 5B). For instance, at  $\varepsilon$ =0.05 the average tangent moduli for freshly harvested E16.5 was 0.729  $\pm$  0.803 MPa, whereas the average for decellularized E16.5 tendons was 0.033  $\pm$  0.033 MPa, indicating high variability based on the standard deviation. Similarly, at  $\varepsilon$ =0.25 the average tangent moduli were 26.166  $\pm$  24.178 MPa for the freshly harvested E16.5 tendons and 0.363  $\pm$  0.145 MPa for the decellularized E16.5 samples. The evaluation of embryonic decellularized tendons with a two-way ANOVA showed a significant increase in moduli as a function of development. Multiple comparisons indicated significant differences in the tangent moduli between individual groups of E16.5 and E18.5 tendons at strain values greater than 0.1 (Fig. 5C).

Further, regional variability in tangent moduli was observed for E16.5 decellularized tendons. The stress-strain response indicated the stiffness of the tendon at the distal region was greater than the mid and proximal ends (Fig. 6A). Two-way ANOVA indicated both strain value and region along the tendon had a significant effect on the tangent moduli of E16.5 decellularized TA, indicating nonlinear behavior (Fig. 6B). Two strain values were then compared, actuator strain and optical strain. Actuator strain was calculated from the displacement imposed by the FemtoTools micromanipulator. Optical strain was calculated from the average distance between fiducial lines that were photobleached onto the sample from videos acquired during uniaxial tensile tests. The importance of using fiducial makers to evaluate strain for soft materials is highlighted by the differences between actuator and optical strain for E16.5 and E18.5 tendons and fibronectin sheets (Supplemental Fig. 7). For example, at  $\varepsilon$ =0.15 the tangent modulus based on optical strain (0.970 MPa) was more than 25-fold greater than that based

on the actuator strain (0.038 MPa) for a freshly harvested E16.5 tendon.

#### 4. Discussion

In this study, we designed a modular device capable of assessing the mechanical behavior of soft biomaterials and showcased the ability of the system to mechanically characterize embryonic tissues at different developmental timepoints. We customized a commercially available micromanipulator with a force resolution of 5 nN - 50 µN and a displacement sensing range starting at 5 nm, facilitating the application of displacements on small samples while recording force. The modularity and small footprint of the system allowed testing under a dissecting microscope to enable the calculation of optical strain (Fig. 1A). Our data demonstrate the capability of the FemtoTools micromanipulator and spring system to resolve the force of samples by subtracting the contribution of the spring itself (Fig. 2A). The system was validated by mechanically characterizing Solaris, a reference material with known material properties (Fig. 2B,C). The spring design was modified to measure the tensile response of fibronectin sheets, fibrin gels, and embryonic tendons. The modularity of the system allowed us to test tissues of different stiffnesses and sizes and can be used to mechanically characterize soft biomaterials and small tissues to obtain physiologically relevant design parameters for scaffolding that seek to emulate native tissue mechanics.

When considering a testing system, the force resolution, maximum force capacity, and the gauge dimensions determine the tissues that can be tested with the system. Force and displacement curves showed minimal noise in unfiltered data (Fig. 4), eliminating the need for processing through filtering and noise-reducing algorithms. The appropriately sized 3D printed spring and microforce sensor with sufficiently high force threshold were selected according to the material size and estimated stiffness prior to tensile testing. When testing developing tissues that change in size and stiffness as a function of development, the adaptability of the system and the force resolution are critical. The force sensing capability of the FemtoTools microsensors is between 100 µN maximum with 5 nN resolution and 100,000 µN maximum with 50 μN resolution. A limitation of this system is measuring tissues that require larger forces, e.g., adult tibialis anterior tendons. Since there are commercially available tensile systems that operate outside of the FemtoTools force threshold, a combination of instruments will be necessary to fully characterize tissues across development. Alternatively, a load element with a larger range can be incorporated with the FemtoTools micromanipulator, an option we are currently pursuing. Adapting to different geometries was feasible given the ease of fabrication through 3D printing of springs and laser cutting of PET frames. The modularity of the system will enable future multiscale studies given that the micromanipulator system can be coupled with the microscope of choice (e.g., dissecting, confocal) to investigate deformation at a range of scales. The ability to use the same instrument for tensile testing at different scales can facilitate meaningful studies relating the microand macroscales. While commercially available bioreactor systems such as the BioTense Perfusion Bioreactor System (Admet) include similar features (e.g., mounting on a microscope, bath, application of uniaxial force, actuator control), the focus on the cellular scale may lead to limitations with mechanically characterization at the tissue scale, especially with larger samples [52]. Further, for the ex vivo mechanical testing of decellularized or immunostained tissues, there is little need for bioreactor features such temperature control and maintaining concentration of nutrients through perfusion.

The results obtained for the elastomer Solaris were similar to those reported by others and by the manufacturer [43,53]. There was a discrepancy in the tangent moduli at  $\varepsilon \leq 0.1$ , where the

bulk material testing system recorded a greater modulus. This is attributed to differences in the casting and curing protocols for samples generated for the FemtoTools and TA.XTPlus systems. Samples tested on the FemtoTools were fabricated via spin coating to generate a thin film of uniform thickness, potentially causing shear stress to align Solaris chains influencing the stress-strain response [54]. In contrast, the Solaris for bulk testing was polymerized in a mold and cured for longer at 70°C. Further, the samples tested with the FemtoTools systems were tested while surrounded by PBS, while those tested with the TA.XTPlus were surrounded by air during testing. Independent of fabrication differences, our instrument identified similar tangent moduli for Solaris tested with a bulk material tester. In addition, the material behavior observed for fibronectin sheets and fibrin gel are similar to those previously published, where the fibrin gels were linear elastic while fibronectin sheets were viscoelastic [55-57]. The tangent modulus of the fibronectin sheets was comparable to the moduli reported in literature 0.1 - 3.5 MPa [51]; however, the fibrin gels were less stiff than described for individual fibrin fibrils  $1.7 \pm 1.3$  MPa [21,51]. We attribute this discrepancy to differences in fibrin polymerization parameters and that we investigated the mechanics of fibrin in the hydrogel form, rather than individual fibers.

Tendons are responsible for transferring the force produced by the muscle to the skeleton with high fidelity while avoiding musculoskeletal injury. Uniaxial tensile testing is most commonly used to characterize the bulk mechanical properties of adult tendon. Adult tendons are predominantly made up of ECM, whereas developing tendons have a substantially higher number of cells. In addition, embryonic tendons are much smaller, making it challenging to test using the standard instrumentation designed to handle larger, stiffer tissues. Given the challenges in isolating and testing embryonic murine tendons under tension, the mechanics of developing tendons are often studied using indentation modalities at the nano and microscales [16,17]; however, this is not the way in which tendons are typically loaded in vivo. The capabilities of our system enabled the characterization of embryonic murine tendon mechanics as a function of development based on uniaxial tensile loading and optical strain. As expected, tendons show viscoelastic behavior, as seen in the stress relaxation test and hysteresis when unloading (Fig. 4A,B). Tangent moduli calculated for E16.5 and E18.5 tendons significantly increased in stiffness as a function of development and varied regionally (Fig. 5A,C; Fig. 6), as previously demonstrated for rat and mouse tendons [27,42,58]. These data demonstrate our experimental and image processing methods can be reliably used to investigate the regional mechanics of small developing tissues.

The variability of tangent moduli among samples within a developmental timepoint could be due to biological variability. Further, the process of attaching tendons to PET frames could affect the mechanical behavior if glue was to cure onto the tendon surface. Future work will need to evaluate a larger sample sizes for each developmental timepoint to compensate for biological variability. This attachment mechanism will need to be further evaluated, since most of the samples tested failed at the muscle insertion and slipping was often observed by dips in the force measurements recorded during testing [36]. This is attributed to a weak interface between the muscle surface and the glue. Slipping was one of the main factors that contributed to the differences between the actuator and optical strain (Supplemental Fig. 7). Future studies will investigate additional ways to secure the full thickness of the muscle tissue without compromising the integrity of the tendon, such as using a UV-curable glue that is more viscous or polymerizes more quickly in order to minimize the risk of the glue wicking onto the tendon surface while attaching the sample to the PET frame. Additionally, different attachment mechanisms that physically prevent the muscle surface from moving and slipping at the glue interface will be explored such as adding enclosures to the PET frames that facilitate completely immersing the muscle in an adhesive, rather than partially covering the muscle with adhesive. While gluing the tendon tissue directly to the frames may be more effective at minimizing slipping at the muscle interface, as is done in many studies, this involves removing the tendon from the native boundary conditions and shortens the overall gauge length, altering the material response during testing. In addition, the use of PET as a frame material may contribute to differences in actuator and optical strain. Future studies will determine the magnitude of deformation of PET and if the material properties are nonlinear within the regime we are testing, which may also affect the force measurements.

Notably, decellularization decreased the stiffness of embryonic tendons, as cells and intracellular proteins are removed. While cells are thought to minimally contribute to the mechanics of adult tendons, there was a significant decrease in the moduli of decellularized embryonic tendons (Fig. 5B). In addition, it appears that the regional variability is not due only to the cells but also the ECM as that is maintained after decellularization (Fig. 6). The residual cellular debris potentially present in the samples (e.g., DNA) could potentially contribute to the mechanical response of the decellularized tissues, and therefore future work would need to look at removing residual DNA to look at the ECM mechanical response in these tissues [59].

Although the mechanical contribution of the spring has been shown to not drastically change over time (Supplemental Fig. 4), it was still necessary to adjust for the spring contribution based on data collected the same day as mechanical testing to account for potential variations. Even after 360 tensile tests conducted over a 21-week period, there was no need to replace the spring due to material fatigue from cyclic testing. However, since we have not considered all potential testing conditions, we recommend regularly performing baseline tests of the spring, and discontinuing use if the baseline force-displacement response becomes irregular. The material properties of the springs are likely affected by polymer melting, resolution of 3D printing, and post-processing of each part. The tensile modulus of the 3D printed spring was orders of magnitude lower than that reported by the manufacturer [60]. This discrepancy needs further investigation to determine the effect of post-processing and printing orientation. Although the influence of aqueous solutions on the mechanical properties of the spring (Supplemental Fig. 5) was consistent and repeatable the mechanism by which PBS contributes to decreased spring stiffness will need to be further investigated. Future iterations of this system will utilize different materials such that the presence of PBS will not influence mechanical properties of the testing system.

#### 5. Conclusion

These data show the ability of our system to characterize a variety of soft biomaterials and small tissues with different material properties. Mechanical characterization of tissues and ECM is vital for understanding the cellular microenvironment during growth and development. The small size and susceptibility to damage of embryonic tissues and soft biomaterials limit the use of tensile testing modalities typically used for adult soft tissues. This testing system can help better understand the mechanical properties of multifunctional ECM polymers, like fibrin and fibronectin, and the mechanical influence of these polymers during tissue growth and remodeling that are currently not completely understood. By quantifying the material properties of soft biomaterials and small tissues, physiologically relevant parameters can be provided for the design and fabrication of regenerative therapies that aim to restore tissue functionality.

# **Declaration of Competing Interest**

The authors declare that they have no known competing financial interests or personal relationships that could have appeared to influence the work reported in this paper.

#### Acknowledgements

This work is supported by NIH R01 AR071359, NIH DP2 AT009833 and NSF CMMI 1911346 to S.C. The authors would like to thank Drs. Jacqueline Linnes and Elizabeth Phillips for assistance with laser cutting, Dr. David Umulis for the use of the Zeiss 800 upright confocal microscope, and Norvin Bruns for fabricating custom mounts and fixtures.

#### Supplementary materials

Supplementary material associated with this article can be found, in the online version, at doi:10.1016/j.actbio.2021.07.035.

#### References

- J.K. Mouw, G. Ou, V.M. Weaver, Extracellular matrix assembly: a multiscale deconstruction, Nat. Rev. Mol. Cell Biol. 15 (2014), doi:10.1038/nrm3902.
- [2] N.D. Murchison, B.A. Price, D.A. Conner, D.R. Keene, E.N. Olson, C.J. Tabin, R. Schweitzer, Regulation of tendon differentiation by scleraxis distinguishes force-transmitting tendons from muscle-anchoring tendons, Development 134 (2007) 2697–2708, doi:10.1242/dev.001933.
- [3] C.C. Banos, A.H. Thomas, C.K. Kuo, Collagen fibrillogenesis in tendon development: Current models and regulation of fibril assembly, Birth Defects Res. Part C Embryo Today Rev. 84 (2008) 228–244, doi:10.1002/bdrc.20130.
- [4] K.C. Clause, T.H. Barker, Extracellular matrix signaling in morphogenesis and repair, Curr. Opin. Biotechnol. 24 (2013) 830–833, doi:10.1016/j.copbio.2013.04.
- [5] D.E. Discher, P. Janmey, Y.L. Wang, Tissue cells feel and respond to the stiffness of their substrate, Science 310 (2005) 1139–1143, doi:10.1126/science.
- [6] C. Bonnans, J. Chou, Z. Werb, Remodelling the extracellular matrix in development and disease, Nat. Rev. Mol. Cell Biol. 15 (2014) 786–801, doi:10.1038/nrm3004
- [7] M.W. Pickup, J.K. Mouw, V.M. Weaver, The extracellular matrix modulates the hallmarks of cancer, EMBO Rep 15 (2014) 1243–1253, doi:10.15252/embr. 201439246.
- [8] D.E. Birk, E.I. Zycband, S. Woodruff, D.A. Winkelmann, R.L. Trelstad, Collagen fibrillogenesis in situ: Fibril segments become long fibrils as the developing tendon matures, Dev. Dyn. 208 (1997) 291–298, doi:10.1002/(SICI) 1097-0177(199703)208:3(291::AID-AJA1)3.0.CO;2-D.
- [9] H.L. Ansorge, S. Adams, D.E. Birk, L.J. Soslowsky, Mechanical, Compositional, and Structural Properties of the Post-natal Mouse Achilles Tendon, Ann. Biomed. Eng. 39 (2011) 1904–1913, doi:10.1007/s10439-011-0299-0.
- [10] N.R. Schiele, J.E. Marturano, C.K. Kuo, Mechanical factors in embryonic tendon development: Potential cues for stem cell tenogenesis, Curr. Opin. Biotechnol. 24 (2013) 834–840, doi:10.1016/j.copbio.2013.07.003.
- [11] W.P. Daley, S.B. Peters, M. Larsen, Extracellular matrix dynamics in development and regenerative medicine, J. Cell Sci. 121 (2008) 255–264 https://doi. org/10.1242/jcs.006064.
- [12] B.K. Connizzo, S.M. Yannascoli, L.J. Soslowsky, Structure–function relationships of postnatal tendon development: A parallel to healing, Matrix Biol. 32 (2013) 106–116, doi:10.1016/J.MATBIO.2013.01.007.
- [13] A.R. Ocken, M.M. Ku, T.L. Kinzer-Ursem, S. Calve, Perlecan knockdown significantly alters extracellular matrix composition and organization during cartilage development, Mol. Cell. Proteomics 19 (2020) 1220–1235 mcp.RA120.001998, doi:10.1074/mcp.ra120.001998.
- [14] J.E. Wagenseil, C.H. Ciliberto, R.H. Knutsen, M.A. Levy, A. Kovacs, R.P. Mecham, Reduced Vessel Elasticity Alters Cardiovascular Structure and Function in Newborn Mice, Circ. Res. 104 (2009) 1217–1224 https://doi.org/10.1161/ CIRCRESAHA.108.192054.
- [15] L. Carta, L. Pereira, E. Arteaga-Solis, S.Y. Lee-Arteaga, B. Lenart, B. Starcher, C.A. Merkel, M. Sukoyan, A. Kerkis, N. Hazeki, D.R. Keene, L.Y. Sakai, F. Ramirez, Fibrillins 1 and 2 perform partially overlapping functions during aortic development, J. Biol. Chem. 281 (2006) 8016–8023, doi:10.1074/jbc. M511599200.
- [16] J.E. Marturano, J.D. Arena, Z.A. Schiller, I. Georgakoudi, C.K. Kuo, Characterization of mechanical and biochemical properties of developing embryonic tendon, Proc. Natl. Acad. Sci. USA. 110 (2013) 6370–6375, doi:10.1073/pnas. 1300135110.
- [17] X.S. Pan, J. Li, E.B. Brown, C.K. Kuo, Embryo movements regulate tendon mechanical property development, Philos. Trans. R. Soc. Lond. B. Biol. Sci. 373 (2018) 20170325, doi:10.1098/rstb.2017.0325.

- [18] N.S. Kalson, D.F. Holmes, A. Herchenhan, Y. Lu, T. Starborg, K.E. Kadler, Slow stretching that mimics embryonic growth rate stimulates structural and mechanical development of tendon-like tissue in vitro, Dev. Dyn. 240 (2011) 2520–2528, doi:10.1002/dvdy.22760.
- [19] A. Subramanian, T.F. Schilling, Tendon development and musculoskeletal assembly: emerging roles for the extracellular matrix, Development 142 (2015) 4191–4204 https://doi.org/10.1242/dev.114777.
- [20] C.J. Miller, L.A. Davidson, The interplay between cell signalling and mechanics in developmental processes, Nat. Rev. Genet. 14 (2013) 733–744, doi:10.1038/ nrg3513.
- [21] P.A. Janmey, J.P. Winer, J.W. Weisel, Fibrin gels and their clinical and bioengineering applications, J. R. Soc. Interface. 6 (2009) 1–10, doi:10.1098/rsif.2008.0327.
- [22] R. Pankov, K.M. Yamada, Fibronectin at a glance, J. Cell Sci. 115 (2002) 3861–3863, doi:10.1242/jcs.00059.
- [23] Á. Enríquez, S. Libring, T.C. Field, J. Jimenez, T. Lee, H. Park, D. Satoski, M.K. Wendt, S. Calve, A.B. Tepole, L. Solorio, H. Lee, High-Throughput Magnetic Actuation Platform for Evaluating the Effect of Mechanical Force on 3D Tumor Microenvironment, Adv. Funct. Mater. (2020) 2005021, doi:10.1002/adfm. 202005021
- [24] J.H. Jordahl, L. Solorio, H. Sun, S. Ramcharan, C.B. Teeple, H.R. Haley, K.J. Lee, T.W. Eyster, G.D. Luker, P.H. Krebsbach, J. Lahann, 3D Jet Writing: Functional Microtissues Based on Tessellated Scaffold Architectures, Adv. Mater. 30 (2018) 1707196, doi:10.1002/adma.201707196.
- [25] Z.A. Glass, N.R. Schiele, C.K. Kuo, Informing tendon tissue engineering with embryonic development, J. Biomech. 47 (2014) 1964–1968, doi:10.1016/J. IBIOMECH.2013.12.039.
- [26] N.R. Schiele, J.E. Marturano, C.K. Kuo, Mechanical factors in embryonic tendon development: Potential cues for stem cell tenogenesis, Curr. Opin. Biotechnol. 24 (2013) 834–840, doi:10.1016/j.copbio.2013.07.003.
- [27] S. Calve, I.F. Lytle, K. Grosh, D.L. Brown, E.M. Arruda, Implantation increases tensile strength and collagen content of self-assembled tendon constructs, J. Appl. Physiol. 108 (2010) 875–881, doi:10.1152/japplphysiol.00921. 2009.-Tissue-en.
- [28] J.M. Silva Garcia, A. Panitch, S. Calve, Functionalization of hyaluronic acid hydrogels with ECM-derived peptides to control myoblast behavior, Acta Biomater. 84 (2019) 169–179, doi:10.1016/j.actbio.2018.11.030.
- [29] A. Jorge-Peñas, H. Bové, K. Sanen, M.M. Vaeyens, C. Steuwe, M. Roeffaers, M. Ameloot, H. Van Oosterwyck, 3D full-field quantification of cell-induced large deformations in fibrillar biomaterials by combining non-rigid image registration with label-free second harmonic generation, Biomaterials 136 (2017) 86–97, doi:10.1016/j.biomaterials.2017.05.015.
- [30] X. Xu, Z. Li, L. Cai, S. Calve, C.P. Neu, Mapping the Nonreciprocal Micromechanics of Individual Cells and the Surrounding Matrix Within Living Tissues, Sci. Rep. (2016), doi:10.1038/srep24272.
- [31] A.D. Doyle, K.M. Yamada, Mechanosensing via cell-matrix adhesions in 3D microenvironments, Exp. Cell Res. 343 (2016) 60–66, doi:10.1016/J.YEXCR.2015.10.
- [32] M. Elhebeary, M.A.B. Emon, O. Aydin, M.T.A. Saif, A novel technique for in situ uniaxial tests of self-assembled soft biomaterials, Lab Chip 19 (2019) 1153– 1161, doi:10.1039/c8lc01273c.
- [33] R.B. Svensson, S.T. Smith, P.J. Moyer, S.P. Magnusson, Effects of maturation and advanced glycation on tensile mechanics of collagen fibrils from rat tail and Achilles tendons, Acta Biomater. 70 (2018) 270–280, doi:10.1016/j.actbio.2018.
- [34] C. Jayyosi, N. Lee, A. Willcockson, S. Nallasamy, M. Mahendroo, K. Myers, The mechanical response of the mouse cervix to tensile cyclic loading in term and preterm pregnancy, Acta Biomater. 78 (2018) 308–319, doi:10.1016/j.actbio. 2018.07.017
- [35] X. Ye, Z. Cui, H. Fang, X. Li, A Multiscale Material Testing System for In Situ Optical and Electron Microscopes and Its Application, Sensors 17 (2017), doi:10.3390/s17081800.
- [36] M. Jiang, Z.T. Lawson, V. Erel, S. Pervere, T. Nan, A.B. Robbins, A.D. Feed, M.R. Moreno, Clamping soft biologic tissues for uniaxial tensile testing: A brief survey of current methods and development of a novel clamping mechanism, J. Mech. Behav. Biomed. Mater. 103 (2020) 103503, doi:10.1016/j.jmbbm.2019. 103503
- [37] H.B. Henninger, B.J. Ellis, S.A. Scott, J.A. Weiss, Contributions of elastic fibers, collagen, and extracellular matrix to the multiaxial mechanics of ligament, J. Mech. Behav. Biomed. Mater. 99 (2019) 118–126, doi:10.1016/j.jmbbm.2019.07. 018.

- [38] J.D. Humphrey, D.L. Vawter, R.P. Vito, Quantification of strains in biaxially tested soft tissues, J. Biomech. 20 (1987) 59–65, doi:10.1016/0021-9290(87) 90267-3.
- [39] M.J. Bradshaw, G.A. Hoffmann, J.Y. Wong, M.L. Smith, Fibronectin fiber creep under constant force loading, Acta Biomater. 88 (2019) 78–85, doi:10.1016/J. ACTBIO.2019.02.022.
- [40] R.F. Ker, Mechanics of tendon, from an engineering perspective, Int. J. Fatigue. 29 (2007) 1001–1009, doi:10.1016/j.ijfatigue.2006.09.020.
- [41] F. Fang, S.P. Lake, Experimental evaluation of multiscale tendon mechanics; Experimental evaluation of multiscale tendon mechanics, J. Orthop. Res. 35 (2017) 1353–1365, doi:10.1002/jor.23488.
- [42] E.M. Arruda, S. Calve, R.G. Dennis, K. Mundy, K. Baar, Regional variation of tibialis anterior tendon mechanics is lost following denervation, J. Appl. Physiol. 101 (2006) 1113–1117, doi:10.1152/japplphysiol.00612.2005.-De.
- [43] SolarisTM Product Information | Smooth-On, Inc., (n.d.). https://www.smooth-on.com/products/solaris/ (accessed July 23, 2020).
- [44] M.E. Wale, D.Q. Nesbitt, B.S. Henderson, C.K. Fitzpatrick, J.J. Creechley, T.J. Lujan, Applying ASTM Standards to Tensile Tests of Musculoskeletal Soft Tissue: Methods to Reduce Grip Failures and Promote Reproducibility, J. Biomech. Eng. 143 (2021), doi:10.1115/1.4048646.
- [45] A.V. Sergueeva, J. Zhou, B.E. Meacham, D.J. Branagan, Gage length and sample size effect on measured properties during tensile testing, Mater. Sci. Eng. A. 526 (2009) 79–83. doi:10.1016/j.msea.2009.07.046.
- [46] D. Eyrich, F. Brandl, B. Appel, H. Wiese, G. Maier, M. Wenzel, R. Staudenmaier, A. Goepferich, T. Blunk, Long-term stable fibrin gels for cartilage engineering, Biomaterials 28 (2007) 55–65, doi:10.1016/j.biomaterials.2006.08.027.
- [47] M. Okada, B. Blombäck, Calcium and fibrin gel structure, Thromb. Res. 29 (1983) 269–280, doi:10.1016/0049-3848(83)90039-7.
- [48] S. Jordahl, L. Solorio, D.B. Neale, S. McDermott, J.H. Jordahl, A. Fox, C. Dunlay, A. Xiao, M. Brown, M. Wicha, G.D. Luker, J. Lahann, Engineered Fibrillar Fibronectin Networks as Three-Dimensional Tissue Scaffolds, Adv. Mater. (2019) 31, doi:10.1002/adma.201904580.
- [49] A. Acuna, M.A. Drakopoulos, Y. Leng, C.J. Goergen, S. Calve, Three-dimensional visualization of extracellular matrix networks during murine development, Dev. Biol. 435 (2018) 122–129, doi:10.1016/J.YDBIO.2017.12.022.
- [50] A. Acuna, S.H. Sofronici, C.J. Goergen, S. Calve, In Situ Measurement of Native Extracellular Matrix Strain, Exp. Mech. 59 (2019) 1–15, doi:10.1007/s11340-019-00499-y.
- [51] R.I. Litvinov, J.W. Weisel, Fibrin mechanical properties and their structural origins, Matrix Biol. 60–61 (2017) 110–123, doi:10.1016/j.matbio.2016.08.003.
- [52] Admet, BioTense Perfusion Bioreactor System, (n.d.). https://www.admet.com/ wp-content/uploads/2015/07/ADMET-BioTense-Bioreactor-System-Brochure. ndf
- [53] K.L. Ruedinger, R. Medero, A. Roldań, R. Roldań-Alzate, Fabrication of Low-Cost Patient-Specific Vascular Models for Particle Image Velocimetry, Cardiovasc. Eng. Technol. 10 (2019) 500-507, doi:10.1007/s13239-019-00417-2.
- [54] M. Liu, J. Sun, Y. Sun, C. Bock, Q. Chen, Thickness-dependent mechanical properties of polydimethylsiloxane membranes, J. Micromech. Microeng. 19 (2009) 035028, doi:10.1088/0960-1317/19/3/035028.
- [55] A. Shinde, S. Libring, A. Alpsoy, A. Abdullah, J.A. Schaber, L. Solorio, M.K. Wendt, Autocrine fibronectin inhibits breast cancer metastasis, Mol. Cancer Res. 16 (2018) 1579–1589, doi:10.1158/1541-7786.MCR-18-0151.
- [56] K.A. Jansen, R.G. Bacabac, I.K. Piechocka, G.H. Koenderink, Cells actively stiffen fibrin networks by generating contractile stress, Biophys. J. 105 (2013) 2240– 2251, doi:10.1016/j.bpj.2013.10.008.
- [57] S. Britton, O. Kim, F. Pancaldi, Z. Xu, R.I. Litvinov, J.W. Weisel, M. Alber, Contribution of nascent cohesive fiber-fiber interactions to the non-linear elasticity of fibrin networks under tensile load, Acta Biomater 94 (2019) 514–523 https://doi.org/10.1016/j.actbio.2019.05.068.
- [58] L.K. Wood, E.M. Arruda, S.V. Brooks, Regional stiffening with aging in tibialis anterior tendons of mice occurs independent of changes in collagen fibril morphology, J. Appl. Physiol. 111 (2011) 999–1006, doi:10.1152/japplphysiol.00460. 2011
- [59] P.M. Crapo, T.W. Gilbert, S.F. Badylak, An overview of tissue and whole organ decellularization processes, Biomaterials 32 (2011) 3233–3243, doi:10.1016/j. biomaterials.2011.01.057.
- [60] 3D Systems Solutions, Material Selection Guide for ProJet® MJP 2500 and 2500 Plus VisiJet® M2 MultiJet Printing materials for functional precision plastic and elastomeric parts, (n.d.). https://www.3dsystems.com/sites/default/files/2020-08/3d-systems-visiJet-m2-material-selection-guide-usen-2020-08-20-web.pdf (accessed December 11, 2020).